Proceedings of the II Symposium on Positron Emission Tomography, Kraków, September 21–24, 2014

AX-PET: from Demonstrator towards a Full-Ring Brain Scanner

P. Solevi* on behalf of the AX-PET collaboration
Instituto de Física Corpuscolar (CSIC/UV), Valencia, Spain

Axial PET is a novel PET concept based on axially oriented crystals. The axial orientation of the scintillating elements mitigates the uncertainty in the determination of the depth of interaction and provides a scalable and flexible design than can be adapted to different imaging scenarios. Two Axial PET modules have been fully assembled and characterized at CERN with both point-like and extended sources. The capability of Axial PET to break the trade-off between sensitivity and spatial resolution was successfully demonstrated.

DOI: 10.12693/APhysPolA.127.1462
PACS: 87.57.uk, and 87.57.nf, 29.40.Mc, 29.40.Wk

1. Introduction

In positron emission tomography (PET) both sensitivity and spatial resolution play an essential role in determining the quality of the final image. While sensitivity constrains the number of coincidences and therefore the noise in the reconstructed image, poor spatial resolution compromises the detection capability of small structures. Sensitivity and resolution are strongly correlated at detection level and usually attempts to improve one of the two cause degradation of the second one. Different detector concepts have been developed in the last decade to break such a trade, among them Phoswich scheme, monolithic scintillating crystals, highly pixellated design [1]. Axial PET (AX-PET) suggests a different detector concept to improve both sensitivity and spatial resolution [2]. Long scintillating crystal bars are axially oriented and arranged on different layers mitigating the uncertainty associated to the depth of interaction (DOI) mostly affected by the crystal radial depth. The AX-PET concept will be described in detail through Sect. 2 together with the main experimental results that drove towards the final proof-of-concept. The non-conventional features of AX-PET required additionally a strong investment towards the development of dedicated reconstruction and modeling algorithms. Some examples of the software developed in the framework of the AX-PET project will be provided in Sect. 3.

2. AX-PET: the demonstrator

AX-PET is based on 100 mm long axially oriented LYSO crystals (Prelude 420 from St. Gobain) having a transversal cross-section of 3×3 mm^2. To recover the axial coordinate of the gamma interaction point an array of Wavelength Shifter (WLS, EJ-280-10x from Eljen Technology) strips is placed underneath each crystal layer. One AX-PET module (see Fig. 1) is made of 48 LYSO crystals and 156 WLS strips stacked in six layers. Both WLS strips and LYSO scintillating crystals are individually read-out by Multi-Pixel Photon-Counters (MPPC from Hamamatsu). The individual readout guarantees a good spatial resolution of 2.0 mm (FWHM) in x and y and, together with the WLS hodoscope, a 3D localization of the gamma interaction point. Two identical AX-PET modules have been fully assembled and set in coincidence forming the so named AX-PET demonstrator. A trigger logic sorts coincidences between the two modules. A low energy threshold set at 50 keV is applied to each crystal. All crystals passing the low discriminator are added and a coincidence is formed if each module provides a signal within [400, 600] keV. The data is then read-out via a VME-PC interface into a standard desktop computer.

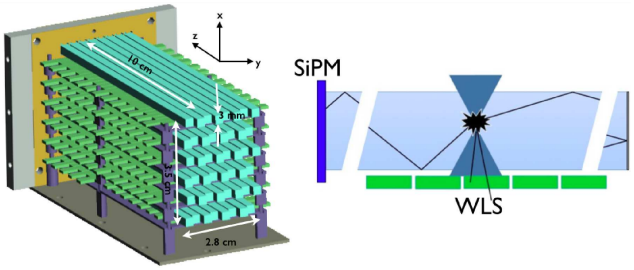

Fig. 1. Left: Schematic drawing of one AX-PET module. In green the WLS strips and in blue the LYSO scintillating crystals. Right: illustration of the AX-PET working principle. The scintillation light produced by the interaction of a gamma photon in the LYSO crystal partly reaches a set of continuous WLS strips. The calculation of the centre of gravity of the signals in the WLS cluster provides the axial coordinate of the gamma interaction.

The AX-PET demonstrator was deeply characterized. In order to estimate the axial resolution, each module was illuminated by a collimated ^{22}Na point-like source. The intrinsic axial resolution achieved for each module was 1.75 and 1.82 mm (FWHM), after applying the proper corrections for acollinearity and positron range. After illuminating each module with a non-collimated ^{22}Na source, a mean energy resolution of 11.8% (FWHM) at 511 keV is obtained averaged over the 96 LYSO crys-

*corresponding author; e-mail: paola.solevi@ific.uv.es

tals. The AX-PET demonstrator was also adapted to image extended sources. For this purpose the two AX-PET modules are placed at 150 mm distance and the phantom placed on a rotating table to allow the data acquisition through different projections. In order to enlarge the field of view (FOV) of the system the relative angle between the modules is changed from 180 to 160 degrees in two consequent tomographic acquisitions. Different phantoms for image quality such as MicroDerenzo, MiniDeluxe and NEMA have been measured.

In Fig. 2 the reconstructed image of the NEMA phantom is provided. Image reconstruction is performed by a maximum-likelihood expectation maximization (ML-EM) with off-line calculation of the system response matrix (SRM) [3]. One of the three sectors of the NEMA phantom consists of five capillaries of different diameters (from 1 to 5 mm). The smallest 1 mm diameter capillary is reconstructed with a resolution of 1.6 mm (FWHM).

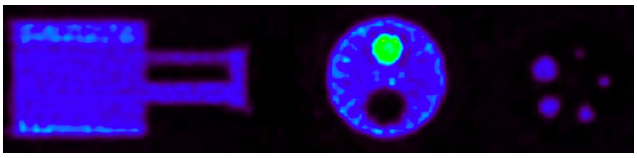

Fig. 2. Reconstructed image of the NEMA phantom at 100 iteration. The NEMA phantom consists of three axial sections: a homogenous background for uniformity studies (left), a homogeneous background region with cold and hot rods (centre), a cold region with five capillaries of different diameters (right).

3. New algorithms for a novel concept

The non-conventional features of AX-PET required dedicated software for image reconstruction and system modeling. For example, the discretized design of AX-PET yields a large number of inter crystal scattering (ICS) that are acquired given the low energy threshold at crystal level and the photopeak selection at the level of the entire module. In an ICS event a photon undergoes a Compton scatter in one scintillating crystal and ends in a photo-electric absorption in another one, see Fig. 3 (top).

These events can represent up to 30% of the total detected coincidences thus it is important to treat them adequately in order to enhance the system sensitivity without spoiling image resolution. An approach that has been studied for AX-PET relies on a better computation of the system matrix elements for such complex events. A detailed description of the technique can be found in Ref. [4]. Images were reconstructed with and without ICS for a rat injected by ^{18}F, as shown in Fig. 3. The reconstructed image obtained with ICS inclusion does not exhibit any resolution loss with respect to the reference image obtained after filtering out ICS coincidences.

A dedicated Monte Carlo model of AX-PET has been developed [5]. Widely validated on experimental data, it represents a valuable synthetic data generator for testing reconstruction algorithms. Additionally simulation studies are ongoing to estimate the performance of an AX-PET full-ring brain scanner (see Fig. 4) in terms of sensitivity, spatial resolution and eventually image quality.

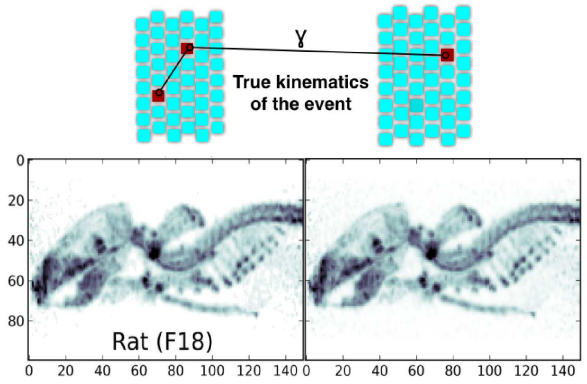

Fig. 3. Top: schematics of an ICS event. One of the photons of the pair interacts in two crystals of one module, through a Compton and a photo-electric interaction. Bottom: rat is injected by ^{18}F and imaged by the AX-PET demonstrator. Images have been reconstructed without (left) and with (right) ICS events. In the imaged rat ICS events increase the number of reconstructed events by about 20%.

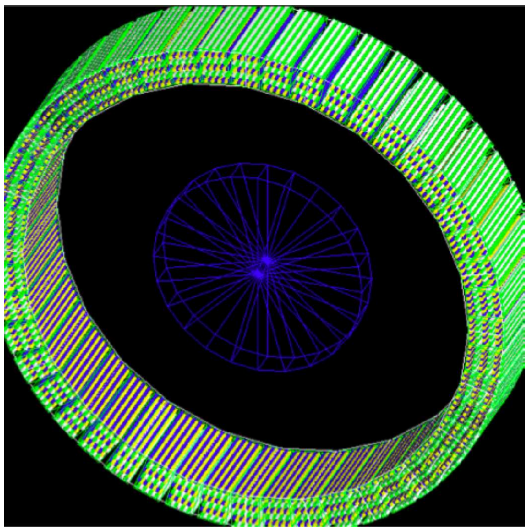

Fig. 4. Simulation screenshot of an AX-PET full-ring scanner. The scanner consists of 48 AX-PET modules arranged in a ring having a diameter of 468 mm.

4. Conclusions and outlooks

The AX-PET demonstrator successfully passed several test stages, first with point-like sources in dedicated laboratory setups and eventually with more complex and extended sources including small animals. The good measured spatial and energy resolutions together with its flexible design made AX-PET a device suitable for different imaging targets. Monte Carlo simulations are ongoing to assess the potential of AX-PET for brain imaging, as originally conceived.

References

[1] C.S. Levin, *J. Nucl. Med.* **53**, 167 (2012).

[2] P. Beltrame, E. Bolle, A. Braem, C. Casella, E. Chesi, N. Clinthorne, R. De Leo, G. Dissertori, L. Djambazov, V. Fanti, M. Heller, C. Joram, H. Kagan, W. Lustermann, F. Meddi, E. Nappi, F. Nessi-Tedaldi, J.F. Oliver, F. Pauss, M. Rafecas, D. Renker, A. Rudge, D. Schinzel, T. Schneider, J. Séguinot, P. Solevi, S. Stapnes, P. Weilhammer, *Nucl. Instrum. Methods Phys. Res. A* **654**, 546 (2011).

[3] P. Beltrame, E. Bolle, A. Braem, C. Casella, E. Chesi, N. Clinthorne, R. De Leo, G. Dissertori, L. Djambazov, V. Fanti, M. Heller, C. Joram, H. Kagan, W. Lustermann, F. Meddi, E. Nappi, F. Nessi-Tedaldi, J.F. Oliver, F. Pauss, M. Rafecas, D. Renker, A. Rudge, D. Schinzel, T. Schneider, J. Séguinot, P. Solevi, S. Stapnes, P. Weilhammer, *IEEE Nucl. Sci. Symp. Med. Imag. Conf. Rec. 2011* Ed. M. Chmeissani, IEEE, Valencia 2011, p. 4411.

[4] J.E. Gillam, P. Solevi1, J.F. Oliver, C. Casella, M. Heller, Ch. Joram, M. Rafecas, *Phys. Med. Biol.* **59**, 4065 (2014).

[5] P. Solevi, J.F. Oliver, J.E. Gillam, E. Bolle, C. Casella, E. Chesi, R. De Leo, G. Dissertori, V. Fanti, M. Heller, M. Lai, W. Lustermann, E. Nappi, F. Pauss, A. Rudge, U. Ruotsalainen, D. Schinzel, T. Schneider, J. Séguinot, S. Stapnes, P. Weilhammer, U. Tuna, C. Joram, M, Rafecas, *Phys. Med. Biol.* **58**, 5495 (2013).